JAAS

ROYAL SOCIETY OF CHEMISTRY

PAPER

View Article Online
View Journal | View Issue

Cite this: *J. Anal. At. Spectrom.*, 2025, **40**, 276

Quantitative sizing of microplastics up to 20 μm using ICP-TOFMS†

Fazzolari Sandro, Hattendorf Bodo and Günther Detlef *

A fundamental study of four different sample introduction systems was carried out to evaluate the upper size limit of microplastics measured by inductively coupled plasma-time-of-flight-mass spectrometry (ICP-TOFMS). Three different, certified microplastic samples (PS, PMMA and PVC) within a size range of 3–20 μm in suspension were measured. In this study, no particles larger than 10 μm could be detected using pneumatic nebulization for sample introduction. However, we were able to extend the upper size limit to 20 μm by either using a falling-tube device or a vertical downwards-pointing ICP-TOFMS. Particle transport efficiencies could only be estimated and were within a range of 13% to 184%. The particle size was quantified by using dissolved citric acid (non-matrix matched) and agreed with reference values. The critical size values were 2.3 μm for PS, 2.4 μm for PMMA and 3.0 μm for PVC. Additionally, in the case of PVC, chlorine could also be detected and the critical size value was 3.9 μm based on the $^{35}Cl^+$ ion signal.

Received 6th September 2024
Accepted 27th November 2024

DOI: 10.1039/d4ja00323c

rsc.li/jaas

Introduction

Since various studies indicated health risks due to the nano- and microplastics that are released into the environment, there is growing interest in developing suitable methods for plastic particle analysis.[1–6] For example, polystyrene (PS) particles have shown pro-inflammatory activity in animal models, while poly(vinyl chloride) (PVC) particles induced the release of inflammatory mediators and caused damage to pulmonary human cells.[5,6] Thus, various analytical strategies are developed for nano- and microplastic characterization, size, mass and concentration determination in a wide variety of matrices.[7] Microplastic analysis has been carried out with optical methods, such as infrared spectroscopy, Raman spectroscopy and microscopy, by mass spectrometry coupled with an atmospheric solid analysis probe (ASAP) or in combination with pyrolysis and gas chromatography (Py-GC)/MS.[8–11] Recently, the use of inductively coupled plasma mass spectrometry (ICP-MS) was proposed for the analysis of microplastic single particles (sp). This approach, which is referred to as sp-ICP-MS, was first proposed by Degueldre *et al.* who operated a quadrupole-based ICPMS, which allowed measurements to be performed at a time resolution of 10 ms for detection of individual particles in transient signals.[12] Sp-ICP-MS provides the possibility to determine the size and the particle number concentration (PNC) for a wide variety of nanoparticles with different element compositions.[13] However, sp-ICP-MS was used only recently for the detection of microplastics. The practical limitations here are the low ionization efficiency of carbon and an elevated background for $^{12}C^+$ signals, arising from the atmospheric nature of the plasma, as contaminants in the argon plasma gas and dissolved carbon species in real-life samples.[7,14,15] The first report on sp-ICP-MS microplastic detection was from Bolea-Fernandez *et al.* who analysed non-functionalized 1 μm and 2.5 μm lanthanide-doped polystyrene (PS) beads.[14] They monitored the $^{13}C^+$ signal and observed that the integrated intensity ratio between 2.5 μm and 1 μm particles closely matched the corresponding particle volume ratio. This indicates that the carbon signal intensity was proportional to the particle volume. Other sp-ICP-MS approaches have also been applied for microplastic measurements.[15–18] For example, Harycki *et al.* performed sp-ICP-TOFMS measurements of metallic nanoparticles and multi-element doped 3.4 μm PS beads.[18] The particles were suspended in simulated sea water at different salt concentrations and quantified using online microdroplet calibration.[18] They also showed that while the particle size determination was not affected by the salt concentration, the critical size value increased with increasing salt content.[18] This indicated that online microdroplet calibration is a promising matrix-matched quantification approach for microplastic analysis in environmental samples such as surface, lake and sea water.[18] The combination of a microdroplet generator (MDG) and pneumatic nebulization system was introduced by Ramkorun-Schmidt *et al.* for the quantification of certified gold and silver nanoparticles.[19] Online microdroplet calibration has been utilized in other studies to determine the particle size and concentration in a matrix-matched quantification approach.[20–23]

ETH Zurich, Department of Chemistry and Applied Biosciences, Vladimir-Prelog-Weg 1, 8093 Zurich, Switzerland. E-mail: guenther@inorg.chem.ethz.ch

† Electronic supplementary information (ESI) available. See DOI: https://doi.org/10.1039/d4ja00323c

Hendriks and Mitrano spiked algae cells with 4 μm-diameter polystyrene particles in microparticle : algae ratios of 1 : 9 and 5 : 9.[17] The authors were able to differentiate polystyrene particles from algae by measuring the elemental fingerprints of phosphorus ($^{31}P^+$) and magnesium ($^{24}Mg^+$) as cell tracers. Furthermore, the authors were able to identify particle:algae heteroaggregates and that the particle populations became more apparent with increasing particle concentration.[17] Van Acker *et al.* analyzed three different microplastics, namely PS, PMMA (poly(methyl methacrylate)) and PVC (polyvinyl chloride), with particle sizes up to 20 μm using laser ablation (LA)-ICPMS.[24] Here the microplastic samples had been lifted from the support surface by a low energy laser pulse and introduced into the plasma. Based on various standard microplastic spheres (PMMA, PS and PVC), a calibration function was created using polymer bead standards which enables the size calibration of different polymers.[24] Vonderach *et al.* analysed 3 μm polystyrene beads in the suspension-approach ICP-TOFMS and determined a particle size of 2.93 ± 0.24 μm using an external calibration with dissolved glucose.[25]

To our knowledge there has been no report of introducing and quantifying particles of 10 μm or larger into the ICP-MS using a suspension-based approach. One of the main limitations of sp-ICPMS or single cell (sc)-ICPMS is the sample transport efficiency, which was found to decrease with increasing particle size.[15,17,26–28] For example, even a so-called high efficiency cell introduction system, specially designed for single-cell analysis, showed that the transport efficiency decreases significantly with increasing cell size.[28] Miyashita *et al.* were able to introduce 2–3 μm cells into the ICP with a transport efficiency close to 100%, which dropped to 86% for 6.4 μm cells.[28] A similar observation was encountered if the high efficiency cell introduction system (HECIS) was used for sp-ICPMS.[15,17] Laborda *et al.* reported a transport efficiency of 29.9% for 2.22 μm PS and 12.5% for 4.82 μm PS particles, respectively.[15] Hendriks and Mitrano achieved a transport efficiency of 77% for 50 nm gold nanoparticles and 20% for 4 μm PS particles.[17] As reported by Olesik and Bates,[29] the commonly used spray chambers remove the majority of droplets >10 μm in size, which obviously also limits the particle sizes that can be transported into the ICP. In order to cope with the challenges encountered during the analyses of microparticles and cells, an ICP-TOFMS with a downward-pointing ICP had been developed.[30] This arrangement allows the introduction of samples with a downward-pointing trajectory regardless of size and mass due to using low gas flows and gravity for sample transport. Initial studies have shown that 100% transport efficiency can be achieved even for droplets up to 93 μm in diameter.[25,30,31]

In this work, aqueous suspensions of 3–20 μm microparticles of different composition were analysed and size quantified using four different ICP-TOFMS configurations. All instrument configurations were studied with a special focus on particle transport capabilities. In addition, quantitative analysis was carried out to determine the size of the particles using non-matrix matched quantification. Finally, figures of merit for all different sample introduction approaches are summarized.

Experimental section

Chemicals and materials

Three different microplastic types were studied, namely polystyrene (PS), poly(methyl methacrylate) (PMMA) and poly(vinyl chloride) (PVC). The physical and chemical properties of the polymers are listed in Table 1.

Particles ranging in size from 3–20 μm (manufacturer values) were purchased from Lab261 (Palo Alto, CA, USA) in 5 mL suspensions with a solid content of 1% in deionized water containing 2 mM NaN_3 as an anti-microbial agent and 0.1% Tween 20 as surfactant. 20 μm PVC was also purchased from Lab261 and additional samples (4 μm and 6 μm PVC from Lab261) were provided by Dr Thibaut Van Acker (Ghent University, Belgium). Prior to all experiments, the microplastic bead samples were inspected by optical microscopy (BX51, Olympus, Shinjuku, Japan) and images were taken using the software "ProgRes CapturePro 2.10.0.1". For the analysis, microplastic suspensions were sonicated for 15 min and diluted in 2% HNO_3 (subboiled in 18.2 MΩ ultrapure water) solution with a particle number concentration (PNC) range as listed in Table S1.† The samples were prepared gravimetrically in conditioned vials. Three aliquots had been prepared for each microparticle sample. Cesium (100 μg mL^{-1}) or aluminium (1000 μg mL^{-1}, both Inorganic Ventures, Christiansburg, VA, USA) were used as droplet tracers to count the number of droplets for setups A and B2 and to determine the aerosol transport efficiency in setups B1 and C.[21]

The carbon quantification was carried out *via* one-point calibration using citric acid monohydrate (Fisher Scientific, Loughborough, UK) in 2% HNO_3 solution. The sensitivity for $^{12}C^+$ was determined either from 500 mg L^{-1} or 1000 mg L^{-1} solutions, respectively, whereas a 5000 mg L^{-1} carbon content was used for determining the $^{13}C^+$ sensitivity.

Methods

All experiments were carried out using four different ICP-TOFMS configurations. One was the prototype downwards-pointing ICP-TOFMS (Fig. 1A).[25,31] The instrument is equipped with a TOF mass analyser (icpTOF R from Tofwerk AG, Thun, Switzerland) coupled to an Elan 6000/6100 (PE/Sciex, Canada) interface with an adapted ICP source. Fig. 1A shows the sample introduction systems of the individual setups which can be divided in three parts: (i) a microdroplet generator (MDG), (ii) a falling-tube device (FTD) with two He gas inlets and (iii) a gas exchange device (GED, J-SCIENCE Lab Co., Ltd, Kyoto, Japan) using argon as sweep gas. The FTD and the GED are used to

Table 1 Chemical and physical properties of the three polymers PS, PMMA and PVC

	PS	PMMA	PVC
Density ρ_P [g mL^{-1}]	1.05	1.18	1.38
Chemical formula of the repeat unit	$(C_8H_8)_n$	$(C_5H_8O_2)_n$	$(C_2H_3Cl)_n$
Carbon concentration c_c [g mL^{-1}]	0.97	0.71	0.53

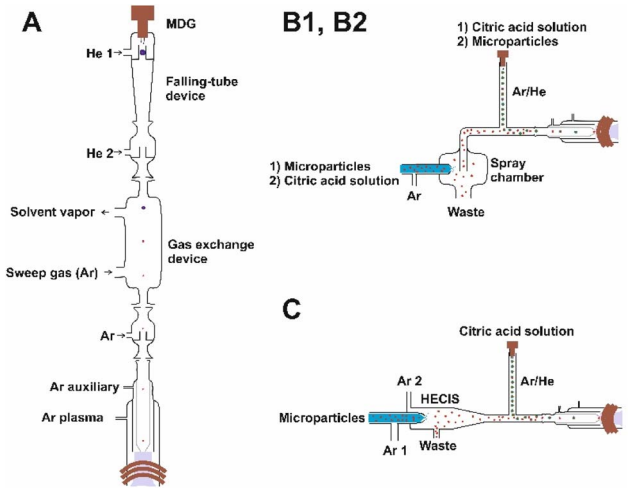

Fig. 1 Schematic sketch of the sample introduction systems used for the downward-pointing ICP-TOFMS (A) and the ICP-TOFMS with horizontal ICP alignment using different particle introduction systems like the cyclonic spray chamber (B1), falling-tube device (B2) and HECIS (C).

reduce the droplet size prior to the introduction into the ICP by solvent evaporation.[30,32] Two MDGs (Microdrop Technologies, Norderstedt, Germany) with nozzle sizes of 50 μm and 70 μm were used. The droplet size was monitored using a CCD camera (MQ013MG-E2, xiQ ximea, Münster, Germany) and UV strobe light. Recording of the droplet size and calculation of the volume was carried out using an in-house written Python program. The monodisperse droplets were recorded to determine the droplet size and volume using an in-house Python program. The 50 μm MDG nozzle generated droplets up to 72 μm and the 70 μm nozzle provided 80 μm sized droplets. The MDGs were used to introduce the calibration solution for the external calibration and the microplastic suspensions into the downwards-pointing ICP-TOFMS. Each sample was measured for 2.5 min and repeated four times to have a total analysis time of 10 min except for the 20 μm particles which were introduced for a period of up to 35 minutes because a lower transport efficiency was observed during the experiments.

In Fig. 1, setups B1, B2 and C show the three other configurations used for the horizontal ICP-TOFMS system (icpTOF2R from Tofwerk AG, Thun, Switzerland). Setup B1 was based on pneumatic nebulization for particle introduction and using the online microdroplet calibration for quantification.[21,23] The second approach used the same setup; however, the particles were introduced *via* the 50 μm MDG (Microdrop Technologies, Germany) into the falling-tube. The calibration solution was then introduced using the pneumatic nebulizer (Fig. 1B2). The third approach was identical to the second but the cyclonic spray chamber had been exchanged for a high efficiency cell introduction system (HECIS) (Elemental Scientific, Omaha, NE, USA) (Fig. 1C). A 500 mg L^{-1} C solution was also used for quantification.

The operating conditions for the microplastic measurements were optimized for maximum $^{12}C^{+}$ sensitivity. The single-ion-signal histogram was collected for the compound Poisson critical value expression.[33]

Table 3 The microparticle measurements in the icpTOF using the pneumatic nebulizer or falling-tube setup for sample introduction

Parameters	Conditions
MDG (50 μm, AD-KH-501-L6, S/N: 78)	Piezo voltage: 48 V, pulse width: 21 μs
Dispensing frequency [Hz]	50
Ar/He gas mixture [L min^{-1}]	0.75 (Ar) and 0.54 (He)
Ar nebulizer [L min^{-1}]	0.75
Ar auxiliary [L min^{-1}]	0.8
Ar plasma [L min^{-1}]	16
Plasma power [W]	1550
MCP voltage [V]	2040
Time resolution [ms]	3.02

Table 2 Parameters used for the analysis of microplastics in the downward-pointing ICP-TOFMS

Parameters	Conditions
MDG (70 μm, MD-K-150-020, SN: 218)[a]	Piezo voltage: 74–75 V, pulse width: 24 μs
MDG (50 μm, MD-K-150, SN: 217)[b]	Piezo voltage: 92 V, pulse width: 24 μs
Dispensing frequency [Hz]	50
He 1 [L min^{-1}]	0.58–0.77
He 2 [L min^{-1}]	0.52–0.67
Ar (sweep gas) [L min^{-1}]	0–0.09
Ar [L min^{-1}]	0.41–0.62
Ar auxiliary [L min^{-1}]	1.46
Ar plasma [L min^{-1}]	14.1–15.8
Plasma power [W]	900
Einzel lens voltage [V]	5
MCP voltage [V]	2030–2100
Time resolution [ms]	3

[a] The 70 μm MDG was operated for the first two batches. [b] The last batch was introduced with the 50 μm MDG to study if a smaller nozzle-sized MDG can introduce particles up to 20 μm. The piezo voltage and the pulse width for both MDGs were adjusted using the control unit MD-E-3021 SN: 0154 from microdrop Technologies GmbH, Norderstedt, Germany

The operating conditions for the downward-pointing ICP-TOFMS prototype are listed in Table 2.

The measurement conditions for the horizontal icpTOF are listed in Table 3. All the particle measurements were carried out using a total analysis time of 182 s for the spray chamber systems and 600 s when using the falling-tube. The icpTOF was optimized to achieve high sensitivity for low mass elements (m/z < 80) and thus, Al was chosen as a droplet tracer.

The measurement conditions for the microparticle measurement using the HECIS (high efficiency cell introduction system designed for TOFWERK) spray chamber are listed in Table 4. The HECIS spray chamber was provided by Dr Kharmen Beham Billimoria (LGC, UK).

Data evaluation

The compound Poisson critical values were obtained by using the collected SIS histogram (saved as a txt-file) in the Labview program "Lc-Ld_Expression-Calc_ver1.0 (1)" which has been made freely available by Gundlach-Graham and Lancaster.[34] The false-positive rate α was set to 1% to obtain the critical values for the split-event correction ($L_{SE,i}$) and 0.01% for the particle-derived critical value ($L_{SP,i}$).[34,35] The critical values were obtained from the Monte Carlo simulated TOF count signals.[34] The corresponding gross signal critical values ($S_{SE,i}$ and $S_{SP,i}$) were derived by adding the critical values to the mean background intensity in counts (λ_i). Split-event correction means that the adjacent data points are summed together only if their signal intensity was above the threshold $S_{SE,i}$. Transient signals, whose signal intensity was above the threshold $S_{SP,i}$, were counted as particle events.[34] All further data evaluation was carried out in Matlab R2021 a.

Downward-pointing ICP-TOFMS: quantification of particle size, volume and transport efficiency

The absolute sensitivity S_i (counts per g) was calculated according to eqn (1).

$$S_i = \frac{I_i}{c_i \times V_D} \quad (1)$$

Table 4 Measurement conditions using the HECIS spray chamber and falling-tube setup for microparticle introduction in the ICP-TOFMS with horizontal ICP alignment

Parameters	Conditions
MDG (50 μm, AD-KH-501-L6, S/N: 78)	Piezo voltage: 48 V, pulse width: 21 μs
Dispensing frequency [Hz]	50
Ar/He gas mixture [L min^{-1}]	0.75 (Ar) and 0.4 (He)
Ar 1 (nebulizer) [L min^{-1}]	0.31
Ar 2 [L min^{-1}]	0.22
Ar auxiliary [L min^{-1}]	0.8
Ar plasma [L min^{-1}]	16
Plasma power [W]	1550
MCP voltage [V]	2040
Time resolution [ms]	2.9

I_i is the mean value of the background-corrected ion signal for the analyte (counts), c_i is the concentration of the analyte i in the droplets (g mL^{-1}) and V_D is the mean volume of the calibration droplets (mL).

The microplastic particle volume V_P (eqn (2)) was calculated by dividing the background-corrected particle ion signal I_P ($^{12}C^+$ or $^{13}C^+$, counts) by the sensitivity S_i (counts per g) and the respective carbon concentration c_c (Table 1).

$$V_P = \frac{I_P}{S_i} \times \frac{1}{c_c} \quad (2)$$

The transport efficiency was determined by dividing the calculated PNC (PNC_{calc}) by the final PNC (PNC_{final}) as listed in Table S1.† The PNC_{calc} in these experiments was obtained *via* eqn (3) where N_P is the counted number of particle events, N_D is the counted number of droplets (based on the $^{133}Cs^+$ tracer signal) and V_D is the mean volume of the monodisperse droplets.

$$PNC_{calc} = \frac{N_P}{N_D \times V_D} \quad (3)$$

Results and discussion

Microparticle analysis

Images of the microplastics are shown in Fig. S1–S3.† Most microparticles showed a uniform size distribution and the measured mean values, determined from 9–20 particles, were close to the reference values listed in Table 5. A broader size distribution was observed for the 4 μm PS, 20 μm PS, 4 μm PVC, 6 μm PVC, 10 μm PMMA and 20 μm PMMA, with a relative standard deviation greater than 10%. Furthermore, the measured mean diameter from 4 μm PS, 4 μm PVC and 10 μm PMMA deviated larger than 10% to the reference diameter.

Table 5 Particle sizes determined from microscopic images in comparison to the reference diameter. The reference diameter and corresponding standard deviations are taken from the certificate

Samples	Reference diameter [μm]	Measured [μm]
3 μm PS	3.10 ± 0.01	3.1 ± 0.1
4 μm PS	4.20 ± 0.17	3.5 ± 0.5
6 μm PS	6.05 ± 0.10	6.1 ± 0.1
8 μm PS	8.12 ± 0.12	8.4 ± 0.4
10 μm PS	9.98 ± 0.10	9.9 ± 0.1
20 μm PS	23.33 ± 1.09	22.5 ± 4.0
5 μm PMMA	5.2 ± 0.1	5.4 ± 0.5
6 μm PMMA	6.2 ± 0.2	6.0 ± 0.1
8 μm PMMA	7.52 ± 0.12	7.6 ± 0.1
10 μm PMMA	10.22 ± 0.30	12.3 ± 3.0
20 μm PMMA	20.03 ± 0.81	18.8 ± 2.6
4 μm PVC	3.69 ± 0.18	3.5 ± 0.5
6 μm PVC	5.59 ± 0.51	6.8 ± 1.5
20 μm PVC	20.93 ± 0.89	22.0 ± 2.0

Single-particle analysis

Typical transient signals of the microplastic analyses using the downwards-pointing ICP-TOFMS (setup A) and the falling-tube experiment (setup B2) are shown in Fig. 2 for PMMA particles of different size. The arrival of the individual droplets is detected *via* the $^{133}Cs^+$ signal and a coincident appearance of the $^{12}C^+$ or $^{13}C^+$ transient peaks reveals the presence of the microplastics within a droplet. Occasional occurrence of peaks with doubled intensity of the $^{133}Cs^+$ signal (marked by asterisks) indicates that two droplets were detected within an integration window of 3 ms. In the initial experiments, the sensitivity of the droplet tracer was typically lower and the occurrence of double droplet events higher (Fig. 2A and B), which is assumed to be related to the stabilization of droplet formation over time. In all

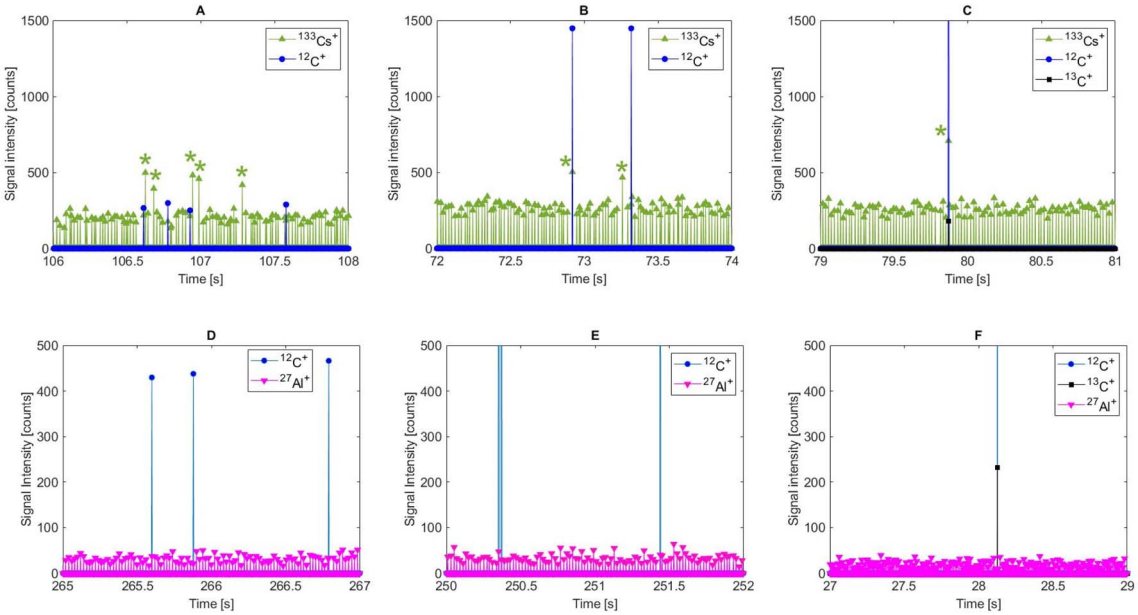

Fig. 2 Transient signals for a period of 2 second from the 5 μm PMMA (A and D), 10 μm PMMA (B and E) and 20 μm PMMA (C and F) measurements with the downward-pointing ICP-TOFMS (A–C) and the setup B2 (D–F). The transient signals were split-event and background-corrected. For each plot, 50 droplets were counted. The dispensing rate was 50 Hz. Asterisks indicate the signals for double droplet events, exceeding a threshold of 5 * σ + μ. The standard deviation σ and the mean value μ were obtained from the Gaussian fits shown in Fig. 3.

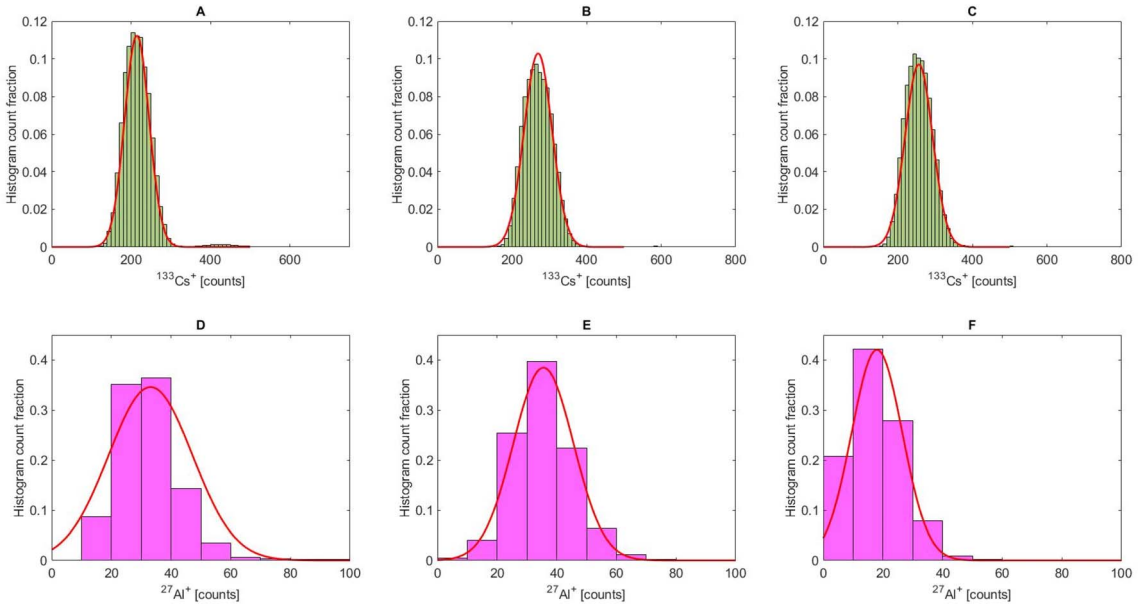

Fig. 3 Histogram of the droplet tracers ($^{133}Cs^+$ and $^{27}Al^+$) from experiments shown in Fig. 2 of the 5 μm PMMA (A and D), 10 μm PMMA (B and E) and 20 μm PMMA (C and F) measurements. The histogram counts were normalized to the total number of droplets injected and fitted with a Gaussian function (red). The bin size was set to 10 counts.

cases however, up to 99.8% of the droplets produced over the course of an experiment could finally be detected in the transient signals and the occurrence of double droplet events was below 1.3%.

The histograms of the droplet signals from these measurements are shown in Fig. 3A–F. The number of droplets in Fig. 3C was higher than that in Fig. 3A and B because the lower transport efficiency for 20 μm particles required a longer measurement time (35 min instead of 10 min) to record at least 40 microparticle events.

Fig. 4A–F show the corresponding particle-derived carbon ion signals of the 5 μm, 10 μm and 20 μm PMMA particles. The signal intensities generally showed a Gaussian distribution except for the 20 μm PMMA (Fig. 4C and F), where 49 microparticles were detected. Additionally, double events have been observed for the smaller particles and even triple events (see Fig. 4A, B and E). The occurrence of double and triple events was below 2% and 0.5%, respectively. The $^{13}C^+$ signal intensity of the 20 μm particle was evaluated for carbon content quantification because the $^{12}C^+$ ion signal exceeded the linear dynamic range of the ion detection system.

Another interesting observation that was made during these experiments was an apparent shift of the signals for droplets containing the microparticles. Especially when introducing droplets with 20 μm particles, we observed that their arrival in the ICP was distinctly offset from the expected time, based on the injection frequency. While "empty" droplets were typically observed to arrive within periods of 20 ms, the particle containing ones frequently appeared at irregular offsets of the expected time, while a gap occurred (*e.g.* at 79.8 s in Fig. 2C) in the

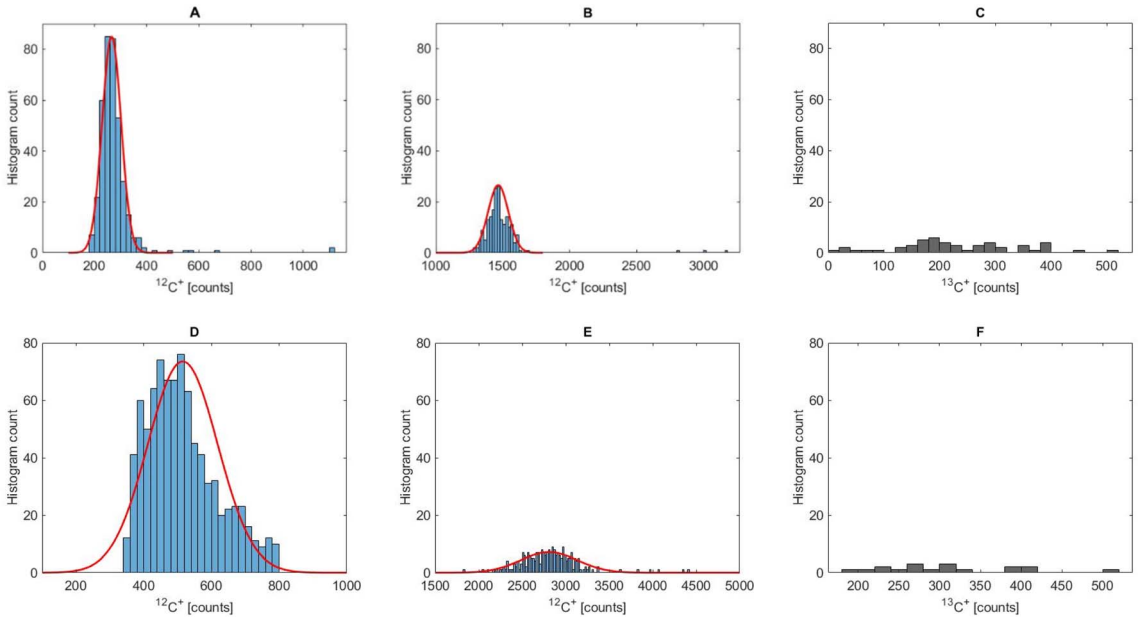

Fig. 4 Histogram of the particle-derived carbon signals from the 5 μm (A and D), 10 μm (B and E) and 20 μm (C and F) PMMA collected from the experiment shown in Fig. 2A–F. The signal distribution was fitted with a Gaussian function. The $^{13}C^+$ ion signal was collected only for the 20 μm particles due to exceeding the linear dynamic range of the $^{12}C^+$ ion signal. The bin size was set to 20 counts.

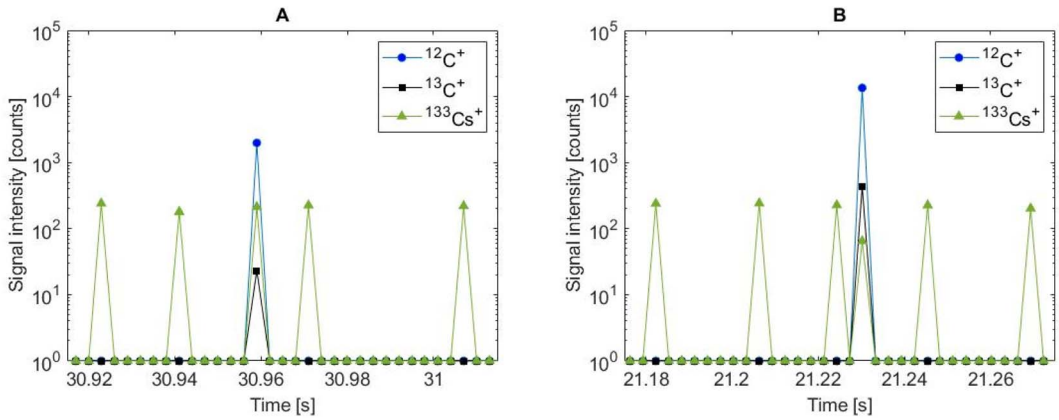

Fig. 5 Transient signals during the injection of 10 μm (A) and 20 μm PS (B) particles into the downwards pointing ICP-TOFMS. The signal suppression of the droplet tracer for the 20 μm PS indicates a more pronounced matrix effect for the larger particles.

droplet tracer signals. It seems that these particles arrived into the ICP at a different flight velocity than the empty droplets. The droplet and particle flight velocities as well as the drying efficiency of various droplet sizes in the downward-pointing ICP-TOFMS need to be further investigated.

Droplets with 20 μm microparticles generally had a lower droplet tracer signal than the 10 μm particles or the empty droplets (Fig. 5), indicating a matrix effect caused by the particles. This was not observed in experiments using the falling-tube setup B2 and seems to indicate that matrix effects were more pronounced for the low plasma power used here.

Particle size determination

Microparticles up to 20 μm could be successfully introduced into the downward-pointing ICP-TOFMS and also in the horizontally aligned ICP using the falling-tube configuration (setup C in Fig. 1) using a droplet generator with 50 μm nozzle size. This supports a finding that the droplet formation is not affected substantially if the suspended particle size is about 5 times smaller than the nozzle size.[36]

The mean particle sizes were determined by considering their stoichiometry and shape *via* the non-matrix matched calibration with all four instrumental configurations. Fig. 6 compares the measured diameters with the reference values provided by the manufacturer. 20 μm particles could in this study only be detected for the downward-pointing plasma and the falling tube setup. Using the cyclonic spray chamber setup, it was furthermore not even possible to introduce the 10 μm particles. Yet an accurate size determination of detected microplastic particles was generally possible with all four methods, indicating that the sensitivity of carbon is practically independent of the composition of the particle and even comparable to that of dissolved citric acid. The uncertainty of the size determination was typically below 15% except for the 20 μm particles when using the falling tube setup. While sizing of microplastics of 8 μm and below seems to be generally possible using pneumatic nebulization with a cyclonic spray chamber, larger particles seem to be not efficiently transported to the ICP. The HECIS can also provide transport of 10 μm particles but the largest sizes were only detected with a vertical arrangement and *via* microdroplet introduction. Critical sizes or size limits of detection were determined from the carbon sensitivities of the different configurations. Due to the differences in carbon concentration in the different materials their critical sizes vary. Using the downward-pointing ICP, the critical size value was 2.3 μm for PS, 2.4 μm for PMMA and 3.0 μm for PVC, respectively. The sensitivity using the horizontal icpTOF2R was higher by a factor of 1.6–2 in comparison to the downward-pointing ICP-TOFMS. However, the $^{12}C^{+}$ background signal was also higher

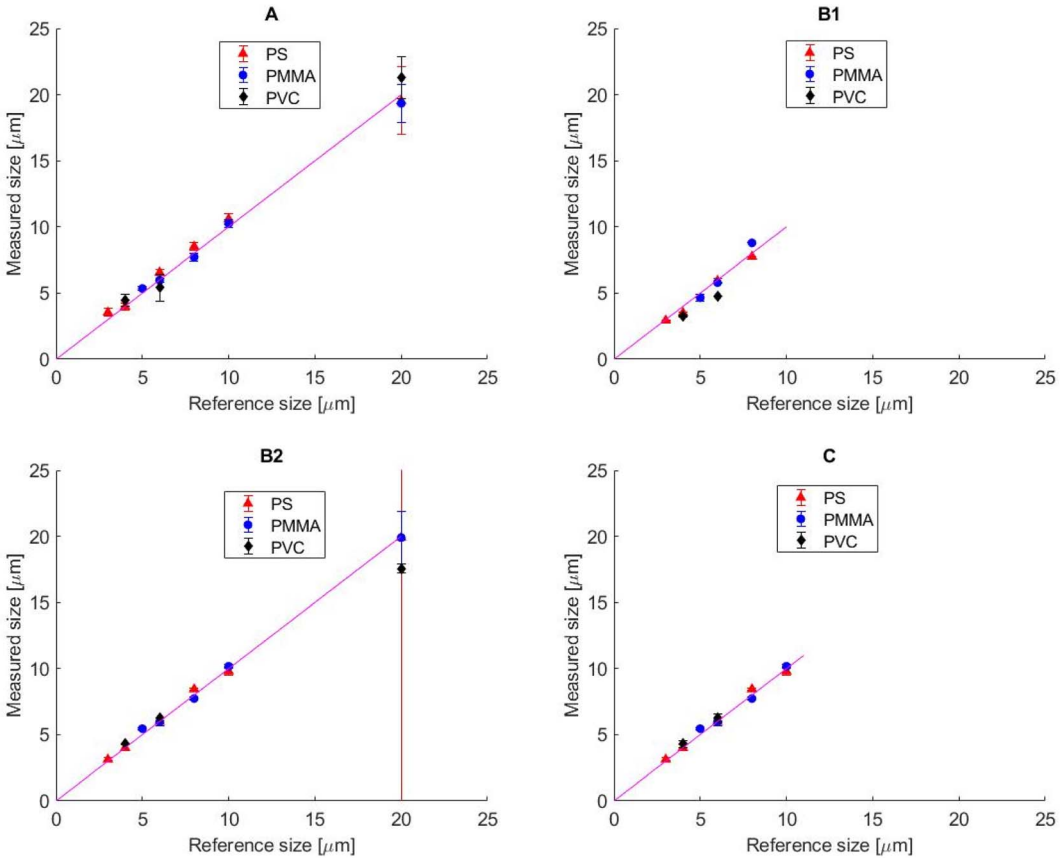

Fig. 6 Comparison of the measured and reference sizes for the different microplastics and sample introduction setups. (A) Downwards ICP, (B1) horizontal ICP using the pneumatic nebulizer and cyclonic spray chamber, (B2) falling-tube and the (C) HECIS. Numerical values are provided in Table S2.† The plots were labeled the same as the four configurations in Fig. 1.

by a factor of 3.7. The critical sizes for the icpTOF2R were thus higher, namely 2.8, 3.2 and 3.8 μm for PS, PMMA and PVC respectively.

Particle transport efficiencies

During analysis of the microplastic suspensions, it was observed that the particle number concentrations obtained for the individual batches varied substantially not only between the different instrumental setups but also within one specific sample type. The resulting mean transport efficiencies are listed in Table 6. There appears to be no correlation between the spread and deviation of transport efficiencies and either particle size or composition at least for the downwards ICP and the falling tube experiments. For experiments with horizontal ICP, the transport efficiencies decreased with increasing particle size, as was reported previously (see Table 6).[14,16,23,24,26] Particles >8 μm could not be detected using the cyclonic spray chamber or with very low numbers for 10 μm microplastics using the HECIS. Initially it was assumed that the large spread in the measured number concentrations (near or above 100% RSD in various experiments) was due to aggregation and/or settling of the particles inside the sample introduction system because dilutions did not contain the same concentration of the stabilizer Tween 20 as the original samples. Yet, samples diluted in the same matrix and measured with downwards ICP and falling tube yielded a similar spread in the particle number concentrations and in part even stronger deviations from the reference values (Table S3†). Due to the fact that particle sizes determined were in agreement with previous measurements, we consider measurement artefacts unlikely.

Table 6 Estimated transport efficiencies (TE) of microparticles obtained from the vertically aligned and the horizontally aligned ICP experiments. Note that the absolute values may be offset due to substantial variations originating in the sample preparation (see text for details)

Sample introduction system, transport efficiency [%]				
		Horizontal ICP		
Sample	Downward-pointing	Cyclonic	HECIS	Falling-tube
3 μm PS	84 ± 57	14 ± 1	49 ± 02	34 ± 06
4 μm PS	72 ± 74	4 ± 1	60 ± 15	25 ± 10
6 μm PS	77 ± 40	1 ± 1	67 ± 12	60 ± 03
8 μm PS	84 ± 13	0.3	26 ± 01	56 ± 06
10 μm PS	90 ± 23	0	10 ± 03	123 ± 30
20 μm PS	38 ± 27	0	0	22 ± 20
5 μm PMMA	25 ± 05	2 ± 1	22 ± 12	57 ± 64
6 μm PMMA	64 ± 19	0.3 ± 0.3	13 ± 05	109 ± 35
8 μm PMMA	115 ± 18	0.2	4 ± 04	80 ± 20
10 μm PMMA	85 ± 35	0	1 ± 01	184 ± 108
20 μm PMMA	62 ± 51	0	0	132 ± 88
4 μm PVC	29 ± 03	2 ± 1	2 ± 01	13 ± 05
6 μm PVC	69 ± 33	0.4 ± 0.2	1 ± 01	14 ± 08
20 μm PVC	43 ± 18	0	0	25 ± 15

Analysing dried droplets of five individual, freshly prepared batches of three microplastic samples of different size by microscopy again revealed a notable spread in particle number concentrations and a deviation of the mean to the reference values by up to a factor of four (Table S4†). This indicates that sample preparation has indeed a substantial impact on the particle number concentrations in the analysed suspension. It is not clear at this stage where these variations originate but it must be concluded that the uncertainty of the determined transport efficiencies is at the order of a factor of two or larger.

Due to the high uncertainties discussed before, it remains difficult to assess whether there is a significant difference in transport efficiencies obtained with the downwards ICP and the falling tube setup for the different sample materials and their sizes. The particle number concentrations determined, however, differ by less than a factor of two from the reference values in most cases, which is in general agreement with the uncertainties observed during sample preparation.

Chlorine detection

A particle-derived chlorine ($^{35}Cl^+$) signal was also observed during the PVC measurements but it was only detected in all

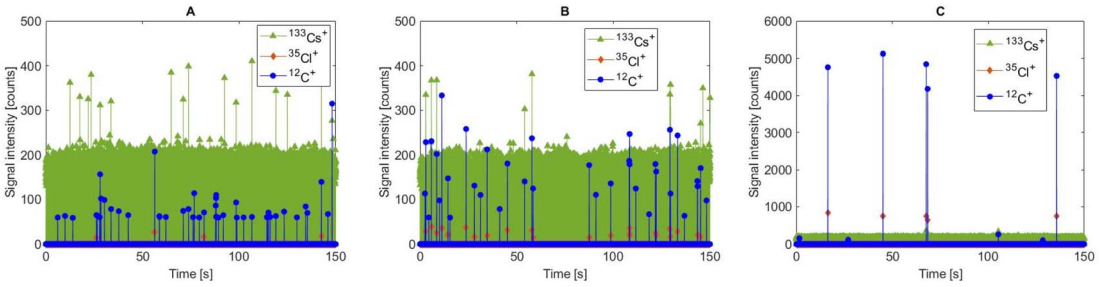

Fig. 7 Transient signals of the 4 μm (A), 6 μm (B) and 20 μm (C) PVC particles showing coincident particle-derived carbon and chloride ion signals.

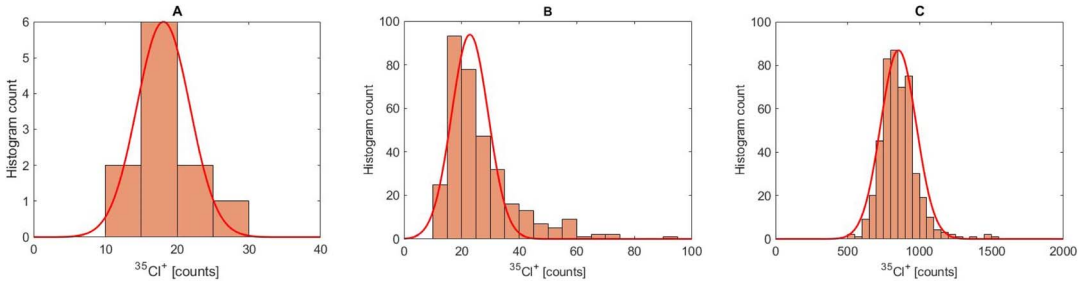

Fig. 8 Histogram of the particle-derived $^{35}Cl^+$ ion signals for 4 μm (A), 6 μm (B) and 20 μm (C) PVC particles with a Gaussian fit function.

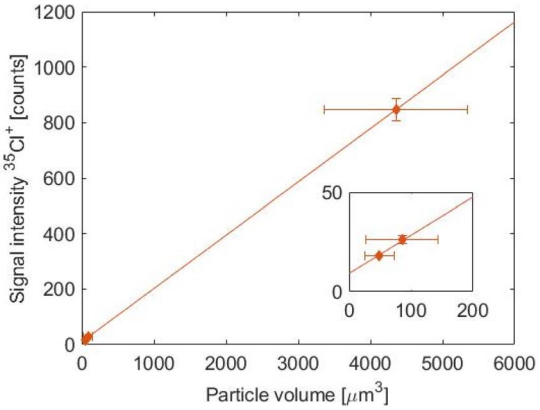

Fig. 9 The chlorine-derived particle ion signal was plotted against the particle volume, determined from the carbon particle mass, to show the linear correlation. The data points of the 4 and 6 μm PVC particles are shown in the smaller plot.

particles for the 20 μm PVC particle (see Fig. 7C). The limited sensitivity of $^{35}Cl^+$, and the elevated background signals on the other hand did not allow its detection in all smaller ones. The particle-derived chlorine signal was only seen in 7% of the total counted particles for the 4 μm PVC and 60% for the 6 μm PVC.

The histograms of the particle-derived chlorine ion signals ($^{35}Cl^+$) are shown in Fig. 8 and fitted by an approximation to a Gaussian distribution. There were also larger signals observed for the 6 μm PVC outside of the Gaussian fit function which might come from larger PVC particles (see Fig. 8B). It was observed from the microscopic images that the 6 μm PVC sample also contained particles up to 9 μm.

Fig. 9 shows a linear correlation of the particle derived chlorine signal with the calculated mean particle volume which was derived from the carbon mass. The critical size value of PVC, based on the $^{35}Cl^+$ sensitivity, was 3.9 μm.

Nonetheless, the experiment demonstrated that also chlorine can be detected in microplastics but only if the particle is sufficiently large like the 20 μm (and partly 6 μm) PVC in this case. The measurement indicated that the applicability of the ICP-TOFMS can be further extended to identify and distinguish chlorinated from non-chlorinated microplastics for particles above 6 μm diameter.

Conclusion

This study compared the applicability of four different sample introduction systems for the analysis of microplastic suspensions with particle sizes up to 20 μm using ICP-TOFMS instrumentation. Pneumatic nebulization with cyclonic or a high-efficiency spray chamber in a conventional horizontal ICP arrangement allowed for successful introduction of suspensions with particle sizes up to 8 μm, while larger particles were not or only poorly (TE ≤ 10%) transported. Using the downward-pointing ICP, the transport efficiency was improved for larger particles substantially and particles up to 20 μm were successfully introduced. Similarly, using the falling tube setup with the horizontal ICP also allowed the introduction of microparticles up to 20 μm. The higher transport efficiency for introduction of the larger microparticles when using vertical droplet injection is most likely a result of better desolvation of the generated droplets, whereby the samples are more efficiently transported with the carrier gas.

Yet, the determination of transport efficiencies for the samples analysed here remained challenging, because the particle number concentration in the analysed suspensions appeared to be affected by the sample preparation. A high variability was obtained for the particle detection events of individual batches of the same sample type and across the different materials and in the absence or presence of Tween 20 as surfactant. Control experiments by microscopy also revealed variations in particle number concentration by approximately a factor of four to the reference values. Therefore, the estimated transport efficiencies are considered to be of similar magnitude. For the spray-chamber based arrangements, the estimated transport efficiencies decreased with increasing particle sizes, which was not the case for the vertical particle introduction. The straight vertical trajectories of droplets and particles for the downward pointing ICP, however, allowed the detection of more particle events per measurement sequence for the largest particle size studied. This is considered to be an advantage for routine applications when analysing microplastic suspensions of unknown size distribution. In all cases where detection was successful, however, the particle sizes could be accurately quantified *via* the $^{12}C^+$ or $^{13}C^+$ ion signals using a standard of dissolved citric acid as the carbon source. Furthermore, the detection of chlorine was also possible for 4 μm PVC particles,

which can be applied to distinguish chlorinated from non-chlorinated microplastics.

Particles of 20 μm diameter were reproducibly detected and size quantified by the vertical droplet and particle injection, suggesting that also larger objects can be analysed with these configurations.

Data availability

The data supporting this article have been included as part of the ESI.† The software "Lc-Ld_Expression-Calc_ver1.0 (1)" from A. Gundlach Graham and R. Lancaster can be found at **https://github.com/TOFMS-GG-Group/Lc-Ld_Expression-Calc**.

Conflicts of interest

There are no conflicts to declare.

Acknowledgements

The first author wants to thank Monique Kuonen, Chiara Fabbretti, Dylan Käser, Tobias Schöberl and Pascal Becker for their contribution. We would also like to acknowledge the LAC workshop for realizing the downward-pointing ICP-TOFMS and the Swiss National Science Foundation (SNSF) for funding *via* project no. 200021_197224.

References

1 S. L. Wright, R. C. Thompson and T. S. Galloway, *Environ. Pollut.*, 2013, **178**, 483–492.
2 T. S. Galloway, M. Cole and C. Lewis, *Nat. Ecol. Evol.*, 2017, **1**, 0116.
3 S.-A. Strungaru, R. Jijie, M. Nicoara, G. Plavan and C. Faggio, *Trends Anal. Chem.*, 2019, **110**, 116–128.
4 J. Zavala, A. N. Freedman, J. T. Szilagyi, I. Jaspers, J. F. Wambaugh, M. Higuchi and J. E. Rager, *Int. J. Environ. Res. Public Health*, 2020, **17**, 1–28.
5 D. M. Brown, M. R. Wilson, W. MacNee, V. Stone and K. Donaldson, *Toxicol. Appl. Pharmacol.*, 2001, **175**, 191–199.
6 H. Xu, P. H. M. Hoet and B. Nemery, *J. Toxicol. Environ. Health, Part A*, 2002, **65**, 1141–1159.
7 M. Velimirovic, K. Tirez, S. Verstraelen, E. Frijns, S. Remy, G. Koppen, A. Rotander, E. Bolea-Fernandez and F. Vanhaecke, *J. Anal. At. Spectrom.*, 2021, **36**, 695–705.
8 C. Vitali, R. J. B. Peters, H.-G. Janssen, M. W. F. Nielen and F. S. Rugeeri, *Trends Anal. Chem.*, 2022, **157**, 116819.
9 A. Käppler, M. Fischer, B. M. Scholz-Böttcer, S. Oberbeckmann, M. Labrenz, D. Fischer, K.-J. Eichhorn and B. Voit, *Anal. Bioanal. Chem.*, 2018, **410**, 5313–5327.
10 Y. Zhong, Q. Bao, L. Yuan, J. Liu, Y. Cai and X. Chen, *Polymers*, 2022, **14**, 3888.
11 C. Vitali, H.-G. Jansen, S. R. Ruggeri and M. W. F. Nielen, *Anal. Chem.*, 2023, **95**, 1395–1401.
12 C. Degueldre and P.-Y. Favarger, *Colloids Surf., A*, 2003, **217**, 137–142.
13 M. Resano, M. Aramendia, E. Garcia-Ruiz, A. Bazo, E. Bolea-Fernandez and F. Vanhaecke, *Chem. Sci.*, 2022, **13**, 4436–4473.
14 E. Bolea-Fernandez, A. Rua-Ibarz, M. Velimirovic, K. Tirez and F. Vanhaecke, *J. Anal. At. Spectrom.*, 2020, **35**, 455–460.
15 F. Laborda, C. Trujillo and R. Lobinski, *Talanta*, 2021, **221**, 121486.
16 L. Hendriks, V. M. Kissling, T. Buerki-Thurnherr and D. M. Mitrano, *Environ. Sci.: Nano*, 2023, **10**, 3439–3449.
17 L. Hendriks and D. M. Mitrano, *Environ. Sci. Technol.*, 2023, **57**, 7263–7272.
18 S. Harycki and A. Gundlach-Graham, *Anal. Chem.*, 2023, **95**, 15318–15324.
19 B. Ramkorun-Schmidt, S. A. Pergantis, D. Esteban-Fernandez, N. Jakubowski and D. Günther, *Anal. Chem.*, 2015, **87**, 8687–8694.
20 L. Hendriks, B. Ramkorun-Schmidt, A. Gundlach-Graham, J. Koch, R. N. Grass, N. Jakubowski and D. Günther, *J. Anal. At. Spectrom.*, 2019, **34**, 716–728.
21 K. Mehrabi, A. Gundlach-Graham and D. Günther, *Environ. Sci.: Nano*, 2019, **6**, 3349–3358.
22 S. Harycki and A. Gundlach-Graham, *J. Anal. At. Spectrom.*, 2023, **38**, 111–120.
23 K. Mehrabi, R. Kaegi, D. Günther and A. Gundlach-Graham, *Environ. Sci.: Nano*, 2021, **8**, 1211–1225.
24 T. Van Acker, A. Rua-Ibarz, F. Vanhaecke and E. Bolea-Fernandez, *Anal. Chem.*, 2023, **95**, 18579–18586.
25 T. Vonderach, A. Gundlach-Graham and D. Günther, *Anal. Bioanal. Chem.*, 2024, **416**, 2773–2778.
26 P. Goodall, M. E. Foulkes and L. Ebdon, *Spectrochim. Acta*, 1993, **48B**, 1563–1577.
27 T. Nomizu, S. Kaneco, T. Tanaka, D. Ito and H. Kawaguchi, *Anal. Chem.*, 1994, **66**, 3000–3004.
28 S. Miyashita, A. S. Groombridge, S. Fujii, A. Minoda, A. Takatsu, A. Hioki, K. Chiba and K. Inagaki, *J. Anal. At. Spectrom.*, 2014, **29**, 1598–1606.
29 J. W. Olesik and L. C. Bates, *Spectrochim. Acta, Part B*, 1995, **50**, 285–303.
30 T. Vonderach, B. Hattendorf and D. Günther, *Anal. Chem.*, 2021, **93**, 1001–1008.
31 T. Vonderach and D. Günther, *J. Anal. At. Spectrom.*, 2021, **36**, 2617–2630.
32 J. Koch, L. Flamigni, S. Gschwind, S. Allner, H. Longerich and D. Günther, *J. Anal. At. Spectrom.*, 2013, **28**, 1707–1717.
33 A. Gundlach-Graham, L. Hendriks, K. Mehrabi and D. Günther, *Anal. Chem.*, 2018, **90**, 11847–11855.
34 A. Gundlach-Graham and R. Lancaster, *Anal. Chem.*, 2023, **95**, 5618–5626.
35 A. Gundlach-Graham and K. Mehrabi, *J. Anal. At. Spectrom.*, 2020, **35**, 1727–1739.
36 R. T. Stovel, *Histochem. Cytochem.*, 1977, **25**, 813–820.